New Light on Ancient Enzymes

- *in vitro* CO_2 Fixation by Pyruvate Synthase of *Desulfovibrio africanus* and *Sulfolobus acidocaldarius*

Andreas Witt[1], Roberta Pozzi[1], Stephan Diesch[1], Oliver Hädicke[2], Hartmut Grammel[1]

[1] Hochschule Biberach, University of Applied Science, Biberach, Germany

[2] Max Planck Institute for Dynamics of Complex Technical Systems, Magdeburg, Germany

Corresponding author
Hartmut Grammel
Biberach University of Applied Science,
Karlstr. 11. 88400 Biberach, Germany
Phone: +49 7351 582-436
Fax: +49 7351 582-469
E-mail: grammel@hochschule-bc.de

Running Title: CO_2 fixation with pyruvate synthase

Enzymes: **EC 1.2.7.1.** Pyruvate:Ferredoxin Oxidoreductase

Keywords: CO_2 fixation, pyruvate:ferredoxin oxidoreductase, *Desulfovibrio*, *Sulfolobus*, autotrophic pathways, anaerobic sulfate reducing bacteria, extremophilic archaea

Abbreviations

PFOR

pyruvate:ferredoxin oxidoreductase

rTCA

reverse tricarboxylic acid

rAcCoA

reductive acetyl-CoA

DC/HB

dicarboxylate/hydroxybutyrate

HPLC-MS

high performance liquid chromatography – mass spectrometry

IPTG

isopropyl-β-D-thiogalactopyranosid

MV

methyl viologen

Abstract

Two variants of the enzyme family pyruvate:ferredoxin oxidoreductase (PFOR), derived from the anaerobic sulfate-reducing bacterium *Desulfovibrio africanus* and the extremophilic crenarchaeon *Sulfolobus acidocaldarius*, respectively, were evaluated for their capacity to fixate CO_2 *in vitro*. PFOR reversibly catalyzes the conversion of acetyl-CoA and CO_2 to pyruvate using ferredoxin as redox partner. The oxidative decarboxylation of pyruvate is thermodynamically strongly favored, and most previous studies only considered the oxidative direction of the enzyme. To assay the pyruvate synthase function of PFOR during reductive carboxylation of acetyl-CoA, is more challenging and requires to maintain the reaction far from equilibrium.

For this purpose, a biochemical assay was established where low potential electrons were introduced by photochemical reduction of EDTA/deazaflavin and the generated pyruvate was trapped by chemical derivatization with semicarbazide. The product of CO_2 fixation could be detected as pyruvate semicarbazone by HPLC-MS.

In a combinatorial approach, both PFORs were tested with ferredoxins from different sources. The pyruvate semicarbazone product could be detected with low potential ferredoxins of the green sulfur bacterium *Chlorobium tepidum* and of *S. acidocaldarius* whereas CO_2 fixation was not supported by the native ferredoxin of *D. africanus*. Methylviologen as an artificial electron carrier also allowed CO_2 fixation.

For both enzymes, the results are the first demonstration of CO_2 fixation in vitro. Both enzymes exhibited high stability in the presence of oxygen during purification and storage. In conclusion, the employed PFOR enzymes in combination with non-native ferredoxin cofactors might be promising candidates for further incorporation in biocatalytic CO_2 conversion.

Introduction

The enzymatic conversion of carbon dioxide has attracted increasing scientific attention in the last years since it opens a perspective for utilizing the climate gas as an alternative feedstock in future strategies to fight global warming [1–3]. In nature, the majority of CO_2 is fixed by ribulose-1,5-bisphoshate carboxylase/oxygenase (rubisco) in the Calvin-Benson-Bassham (CBB) cycle during photosynthesis of plants, algae and cyanobacteria. The enzyme is however inefficient in terms of turnover number and substrate specificity [4]. Together with its overall high ATP-cost, the CBB cycle may not be a primary candidate pathway for biocatalytic CO_2 conversion [5, 1, 6].

However, the prokaryotic world offers a variety of alternative carboxylating enzymes which are involved in autotrophic or heterotrophic pathways. Many of these enzymes remain largely unexplored in terms of their capacity to fix CO_2 *in vitro*.

In the present study, we examine CO_2 conversion by two members of the bidirectional enzyme pyruvate:ferredoxin oxidoreductase (PFOR) (EC 1.2.7.1). PFORs are thiamin pyrophosphate (TPP)-dependent, iron-sulfur containing enzymes which reversibly catalyze the interconversion of acetyl-CoA and CO_2 to pyruvate, utilizing ferredoxin as redox cofactor. PFOR is distributed among autotrophic and heterotrophic bacteria as well as apparently all archaea. It is also present in amitochondrial eukaryotic protists [7, 8], including some human protozoan parasites [9, 10]. It is believed that these enzymes existed before the kingdoms eubacteria, archaea and eukaryotes diverged in evolutionary history and was later replaced by the well-characterized pyruvate dehydrogenase (PDH) multi enzyme complex for oxidative decarboxylation of pyruvate in aerobic metabolism. In contrast to PFOR, PDH utilizes NAD^+ as electron acceptor and catalyzes an essentially irreversible reaction. In organisms where PFOR is engaged in pyruvate decarboxylation, the reduction of ferredoxin provides low potential electrons to fuel diverse reductive processes such as nitrogen fixation [11], or hydrogen evolution [12].

On the other hand, PFOR is also involved in three of the currently known six autotrophic pathways in prokaryotes as a CO_2-fixing enzyme by reductive carboxylation of acetyl-CoA. These are the reverse tricarboxylic acid (rTCA) cycle, originally discovered in anaerobic photosynthetic green sulfur bacteria [13], the reductive acetyl-CoA (rAcCoA) pathway of acetogenic bacteria and methanogenic archaea, and the archaeal dicarboxylate/hydroxybutyrate (DC/HB) cycle (reviewed e.g.in [14]). When operating as a

reductive carboxylase, the enzyme is also called pyruvate synthase. From an energetic point of view, the rTCA cycle and the rAcCoA pathway are considered to be more efficient than the CBB cycle [15, 16], thus potentially providing promising enzymes for CO_2 conversion in natural or synthetic pathways. Depending on the direction of the PFOR reaction, ferredoxin serves either as electron acceptor or electron donor. Ferredoxins are small iron-sulfur proteins which transfer electron in numerous biological processes. The structural diversity in iron-sulfur cluster arrangement and protein sequence results in a great variety of standard redox potentials (E^0') of natural ferredoxins covering a span from +500 mV to lower than -500 mV [17]. Since the reduction of CO_2 requires a strong reductant with E^0' of around -540 mV [18], it appears plausible that the oxidative or CO_2-fixing direction of the PFOR reaction is determined primarily by E^0' of the cognate ferredoxin redox partner in the native host organism.

All PFORs are members of the superfamily of 2-oxoacid:ferredoxin oxidoreductase (OFOR) which show a broad substrate specificity towards 2-oxoacids including pyruvate, 2-oxoglutarate, 2-oxobutyrate, 2-oxoisovalerate and indolpyruvate. OFORs are composed as either homodimers, heterodimers, heterotrimers, heterotetramers, or heteropentamers [19] Despite variations in the subunit composition, all PFORs are apparently phylogenetically related and share a similar overall domain architecture with of up to seven domains per monomer. All have in common a TPP binding site in domains I and IV at the active site of the enzyme. TPP performs a nucleophilic attack to the α-carbon of the 2-oxoacid substrate. The catalytic mechanism involves the formation of a stable radical intermediate [18].

For a few members of the OFOR family, the crystal structures have been resolved. The first three-dimensional structure became available for PFOR from the anaerobic sulfate-reducing bacterium *Desulfovibrio africanus* (PFORdaf). PFORdaf is a 260 kDa homodimeric A2-type enzyme composed of seven domains per monomer [20] and houses three [4Fe-4S] clusters, out of which two are arranged in an intramolecular ferredoxin-like domain V (Fig. 1). The midpoint potentials (E^0') of these clusters correspond to -540 mV, -515 mV and -390 mV, respectively [21] and thus are suitable to communicate between the redox potentials of the catalyzed reaction and ferredoxin of *D. africanus* (E^0' = -385 mV) [22]. Together with the spatial arrangement of the clusters these redox potentials suggest an electron transfer pathway where low-potential electrons generated by pyruvate decarboxylation pass along the proximal, the median and the distal cluster [21] to the protein surface where they are transferred to the external ferredoxin redox partner.

The enzyme of *D. africanus* is further exceptional in showing a higher tolerance towards oxygen than most other PFORs which are rapidly and irreversibly inactivated upon air exposure. Protection towards oxygen of PFORdaf is conferred by a disulfide-bond mechanisms and the unique domain VII at the C-terminus of the protein [23].

Recently, another related homodimeric PFOR structure (although no domain VII is present) became available for the acetogen *Moorella thermoacetica* [24].

As a second enzyme, we have chosen a member of the less complex heterodimeric (αβ-type) PFOR of *Sulfolobus acidocaldarius* (PFORsac). *S. acidocaldarius* is an extreme thermoacidophilic crenarchaeon that has become a model organism for many seminal studies of archaeal biology [25]. The organism thrives all around the world in terrestrial geothermal sulfur-containing biotopes at pH 2-3 and 80 °C [26].

The choice for *S. acidocaldarius* was guided by its obligate aerobic lifestyle giving rise to the expectation to find an oxygen-tolerant PFOR here as well. Initially isolated as a facultative autotroph from a solfataric hot spring, the organism is cultivated in the laboratory in most cases under aerobic heterotrophic conditions.

Since PDH is missing in archaea, PFOR is engaged here in the CO_2-releasing conversion of pyruvate to acetyl-CoA during the dissimilation of carbohydrates.

The 3-hydroxypropionate/4-hydroxybutyate cycle, a pathway that does not include PFOR, has been proposed for autotrophic CO_2 fixation in Sulfolobales [27]. Analysis of the genome sequence reveals that all genes for the PFOR-utilizing DC/HB cycle are also present in *S. acidocaldarius*. A contribution of PFORsac to autotrophic growth is however unlikely, since the high redox potential at aerobic conditons prevents the reduction of the ferredoxin cofactor.

PFORsac exhibits a simpler domain architecture than PFORdaf. It lacks an intramolecular ferredoxin domain and only one single [4Fe-4S] cluster is present per αβ structure. Recently, the crystal structure of a heterodimeric αβ type OFOR became available from *S. tokodaii* [19] (Fig. 1) which is closely related to *S. acidocaldarius*.

Only in a few cases, the carboxylating pyruvate synthase activity of PFOR has been demonstrated experimentally. For the two enzymes chosen for the present work, the reversibility of the reaction has not been established up to now *in vitro* in a biochemical assay. While the oxidative direction of PFOR is routinely assayed colorimetrically by reduction of

methylviologen (MV) as artificial electron acceptor, the reductive carboxylating direction is more challenging and requires to keep the reaction out of equilibrium. In most of the previous studies, the pyruvate synthase function of PFOR has been demonstrated by incorporation of radiolabeled $^{14}CO_2$ into pyruvate e.g. [13, 28, 29] because of the high sensitivity of the method. Two studies reported a non-radioactive alternative where the formed pyruvate was converted to lactate by addition of a NAD-dependent lactate dehydrogenase, thus allowing the continuous monitoring of NADH absorbance. This approach however is complicated by the need of a second enzyme for the "upstream" reduction of ferredoxin. In one case, CO dehydrogenase was employed for this purpose to demonstrate pyruvate synthase activity of PFOR of *Clostridium thermoaceticum* [30] and in another study, 2-oxoglutarate:ferredoxin oxidoreductase in an assay with PFOR from *Hydrogenobacter thermophilus* [31]. The setup is however limited for rapid assaying of pyruvate synthase activity since it requires the isolation of a second enzyme and yields mixed kinetic data.

We here provide a non-radioactive alternative for routinely *in vitro* assaying pyruvate synthase without the complication of having a second enzyme at hand. For both chosen enzymes, the present study is the first experimental demonstration of their pyruvate synthase function *in vitro*.

Results and discussion

Heterologous expression of recombinant PFORs

For obtaining PFOR enzymes of *D. africanus* (PFORdaf) and *S. acidocaldarius* (PFORsac), two recombinant expression vectors pET23d(+)*pfordaf* and pET23d(+)*pforsac* were constructed. pET23d(+)*pfordaf* contained a synthetic gene sequence encoding the 130 kDa monomer subunit of the homodimeric enzyme of *D. africanus* (Desaf_2186) [20]. For the heterodimeric PFORsac, sequence analysis of the genome of *S. acidocaldarius* revealed the presence of two gene sets annotated as pyruvate flavodoxin/ferredoxin oxidoreductase (Saci_2306, Saci_2307) and oxoacid:ferredoxin oxidoreductase (Saci_0208, Saci_0209), respectively. For the present study, we chose Saci_2306 and Saci_2307, which share high sequence similarity and domain architecture with the enzyme of *S. tokodaii* for which the crystal structure has been recently resolved [19].

Saci_2306 encodes an α-subunit of 303 amino acids and a theoretical molecular weight of 68.6 kDa. The 303 amino acid β-subunit, encoded by Saci_2307 with a theoretical molecular weight of 33.7 kDa, contains the conserved TPP-binding site.

pET23d(+)*pfordaf* and pET23d(+)*pforsac* were transformed into *E. coli* Tuner^{TM}(DE3) as a host strain for high-level expression using the T7 polymerase expression system. Cultivations were either in shake-flasks or, for large-scale production and in order to have a better control on the cultivation conditions, in a fully automated 10 L stainless steel stirred-tank bioreactor. However, after IPTG-induction of heterologous expression of PFORdaf, we found the major portion of the produced recombinant enzyme insoluble in cellular inclusions bodies. Accordingly, only low specific activities in the MV reduction assay were present in the soluble protein fraction.

Cultivation and expression conditions were subsequently changed to improve the yield of biologically active soluble enzyme and optimized for the expression of PFORdaf. Since three [4Fe-4S] clusters are present in each subunit of A2-type PFOR, the assembly of Fe-S clusters was supposed to be a limiting factor in *E. coli*, preventing larger amounts of functional protein to be synthesized. We therefore changed the expression system to modified host strain, *E. coli* BL21(DE3)*ΔiscR* [32]. The *isc* operon encodes assembly proteins for Fe-S cluster biogenesis in *E. coli* [33]. The strain carries a functional deletion of the IscR repressor protein of the *isc* operon and has been successfully employed previously for heterologous expression of PFORs

of *Chlamydomonas reinhardtii* [12] as well as for recombinant hydrogenases [32]. Recently, expression of PFORdaf using this host strain was also accomplished by another group [34].

As further modifications, after IPTG induction, the cultivation temperature was lowered from 37 °C to 22 °C and the culture was shifted to anaerobic conditions. Aerobic cultivation did not result in any soluble PFORdaf. Together, these measures resulted in a strong elevation of recombinant PFORdaf expression in the soluble fraction of cell lysates (Fig. 2). MV reduction activities in cell lysates obtained with the *E. coli ΔiscR* strain were about 10-fold higher than with the commercial *E. coli* Tuner^{TM}(DE3) strain.

A similar cultivation strategy was applied for expression of recombinant PFORsac (see Material and methods). However, soluble PFORsac could be obtained without switching to anaerobic conditions at a controlled dissolved oxygen value of 30 % air saturation. Possibly, the lower molecular weight and the presence of only one FeS cluster per protein subunit when compared to PFORdaf, facilitates protein folding of PFORsac in the presence of oxygen.

It is at present unclear whether the effect on PFORdaf expression is caused directly by oxygen or more general by lowering the growth and protein biosynthesis rate at anaerobic conditions to facilitate the maturation of the larger and more complex PFORdaf.

After purification by affinity chromatography, electrophoretically homogenous proteins were obtained in both cases with molecular weights of 128 kDa corresponding to the monomer subunit of PFORdaf whereas PFORsac yielded two polypeptides of 71 kDa and 34 kDa, respectively, corresponding to the α/β-subunits of heterodimeric PFORsac (Fig. 2).

Characterization of recombinant PFORs

The highest specific activity for purified recombinant PFORdaf, measured as MV reduction was 72 U mg^{-1} (where 1 U corresponds to 1 μmol pyruvate min^{-1} mg^{-1}). The value is in close agreement with that reported previously for the native enzyme purified from *D. africanus* (70 U mg^{-1} [21]). Varying the pH range from pH 6-9 resulted in the highest activity in Tris/HCl buffer at pH 9.0 also confirming previously published data [21]. However, the data of Pieulle et al., [21] were obtained at an assay temperature of 30 °C. For determination of the temperature optimum of the enzyme, we varied the assay temperature from 25-60 °C and found increasing specific activities at raising temperatures with a maximum at 50-55 °C.

With recombinant PFORsac a lower maximal activity of 10 U mg^{-1} was obtained. Elevation of the reaction temperature revealed an almost linear increase of the *in vitro* activity up to 70 °C

which is in the range of the reported temperature optimum for growth of *S. acidocaldarius*. A discrepancy appeared when determining the pH dependency of the enzyme. *S. acidocaldarius* as a thermoacidophilic crenarchaeon grows optimally at 80 °C and pH 2, whereas the *in vitro* activity of the recombinant enzyme peaked at alkaline pH 10.0. For both, PFORdaf as well as PFORsac, the decarboxylation of pyruvate might be favored at high pH due to the release of a proton and of CO_2 during the reaction. No pH optima have been determined for the reductive carboxylating activity (see below).

For the native PFORdaf, some kinetic data have been published previously including an apparent K_m value for pyruvate of 5.5 mM [21] and we did not re-determine these parameters in the present study. For PFORsac we found a lower apparent K_m for pyruvate of 0.21 mM, in the same order of magnitude as recently reported for the respective enzyme of *S. tokodaii* (K_m = 0.32 mM, V_{max} = 7.5 U mg-1) [19].

The chosen PFORsac did not only show MV-reduction activity with pyruvate but also accepted 2-oxoglutarate as a substrate. However, the enzyme showed a higher preference for pyruvate with a 5.5-fold higher reaction rate then with α-ketoglutarate, so we kept the term PFORsac in the present contribution instead of OFORsac.

For exploiting enzymes in biocatalytic processes, stability is of critical importance. Long-term stability during storage was tested with the MV reduction assay in different buffer compositions, pH values and storage temperatures. Both enzymes exhibited remarkable storage stability even without any protective measures to avoid oxygen. With PFORsac, no decrease compared to the initial activity of purified enzyme was observed during a time period of 32 days when stored in Tris/HCl (20 mM), pH 8.5 at 4 °C. The high storage stability could also be confirmed for PFORdaf. The remarkable robustness of both enzymes during purification and storage makes PFORdaf and PFORsac promising candidates for further development as CO_2-utilizing biocatalysts.

Reductive carboxylation of acetyl-CoA

All enzyme measurements above as well as published data for PFORdaf and PFORsac were using the MV reduction assay and thus only consider the oxidative decarboxylating activity. In contrast, no experimental data for either of the two enzymes, working in the reverse, CO_2-fixing direction as a pyruvate synthase were available up to now. The lack of data is in part due to the fact that no convenient (i.e. simple, non-radioactive) assay is available. In the

current study, we therefore established a biochemical assay for demonstration of the putative pyruvate synthase operation of PFORdaf and PFORsac, respectively.

PFOR reversibly catalyzes the following reaction:

$$CO_2 + \text{Acetyl-CoA} + 2\ Fdx_{red} + H^+ \leftrightarrow \text{Pyruvate} + \text{CoA} + 2\ Fdx_{ox}$$

The conversion of acetyl-CoA and CO_2 to pyruvate is a redox reaction with an estimated reduction potential E^0' = -515 ± 33 mV. The E^0' value was calculated from the individual formation energies of the participating molecular species (acetyl-CoA, CO_2, CoA and pyruvate) (equilibrator.weizmann.ac.il/) [35]. This estimation results in a Gibbs free energy ΔG' = 99.5 ± 6.3 kJ mol^{-1} imposing a thermodynamic barrier upon the reductive carboxylation of acetyl-CoA. (Note that ΔG' refers to 1 mM concentration of all reactants and pH 7.0).

If the concentrations of substrates are higher and product concentrations lower, CO_2 reduction becomes more favorable. However, even with the actual concentrations of substrates (acetyl-CoA, 3.0 mM; CO_2, 23 mM (see below)) and products (here arbitrarily, 10^{-6} mM for initial pyruvate and CoA, respectively) and pH 7.2 applied in our test tube, ΔG' is still positive with 21.6 ± 6.3 kJ mol^{-1}.

Hence, to facilitate CO_2-fixation and reach a negative ΔG value, two conditions should be fulfilled: the reaction system has to be kept in disequilibrium and the ferredoxin redox cofactor should provide high energy (i.e. low redox potential) electrons.

The effective redox potential however, is dependent not solely upon E^0' but also upon the concentration ratio of the reduced and oxidized species, according to the Nernst equation ($E = E^0' + RT/nF \ln[\text{ox/red}]$ (with R: gas constant; F: Faraday constant and n: number of electrons transferred). As a consequence, a negative overall ΔG can be achieved even with midpoint potentials more positive than -515 mV, provided that the electron carrier is in a highly reduced state. A systematic analysis of the thermodynamic relationships between E^0' of the redox cofactor, the reduction grade (reduced/oxidized ratio) of the redox cofactor and ΔG has been conducted and is depicted in Figure 3. From the simulation, two parameter regions separated by the isocline, representing the 99.5 kJ mol^{-1} boundary can be identified. In the parameter space to the left of the isocline, CO_2 fixation is infeasible regardless of E^0' and the reduction grade of the cofactor, while all the parameter combinations on the right site of the isocline, thermodynamically allow CO_2 fixation.

This isocline represents the scenario when all species except the redox cofactor are present with equimolar concentrations of 1 mM. With the applied concentrations of our experimental setup the isocline would be shifted to the left indicating that redox cofactors with even less negative reduction potential and/or lower reduction grades would still be sufficient to drive the carboxylation reaction.

The simulation in Fig. 3 allows to deduce the minimal reduced/oxidized ratio of a given redox cofactor when $E^{0'}$ is known and was used for estimating the actual reduced/oxidized ratio of the redox cofactors employed in the experimental work below.

A high substrate/product ratio can be maintained by coupling further reactions "downstream" and "upstream" of the PFOR reaction as also recently pointed out in Li and Elliott, [34]. In the present assay, outlined in Fig. 4, the upstream reaction continuously regenerates reduced ferredoxin (or MV) by photochemical reduction of EDTA/5-deazaflavin. This part has been adopted from a similar previous approach with heterocyst extracts from cyanobacteria [36]. In the downstream reaction, the generated pyruvate is removed out of the equilibrium by chemical trapping with semicarbazide in an essentially irreversible reaction with a reported first-order rate constant of about 18.5×10^5 $M^{-1}min^{-1}$ [37]. The ultimate pyruvate semicarbazone product of the assay can easily be measured by HPLC. Overall the procedure provides a novel and simple non-radioactive procedure for rapid assaying pyruvate synthase function of PFOR *in vitro*.

Pyruvate synthase activities of PFORdaf and PFORsac were tested in combinations with their cognate ferredoxins (Fdx_daf and Fdx_sac, respectively), and in addition with ferredoxin isolated from *Chlorobaculum tepidum*, (Fdx_cte) a moderate thermophilic green sulfur bacterium and with commercial spinach ferredoxin from *Spinacia oleracea* (Fdx_sol). Alternatively, MV was employed as an artificial redox mediator (Table 1). *C. tepidum* performs anoxygenic photosynthesis at anaerobic conditions and uses the rTCA cycle for autotrophic growth with PFOR being one of the key enzymes [13]. Thus, we know that Fdx_cte is capable of driving CO_2 fixation via PFOR *in vivo*. The use of the cognate PFOR from *C. tepidum* was not considered for the current study since after isolation, this enzyme was rapidly inactivated due to the known high oxygen sensitivity of PFORs originating of the anaerobic rTCA cycle [14].

Two ferredoxins I and II have previously been identified as substrates for PFOR in *C. tepidum* [38]. In the present study, purified ferredoxin I was employed as Fdx_cte. *S. acidocaldarius*

contains a dicluster ferredoxin (Fdx_sac) with a [3Fe-4S] cluster having a midpoint potential ($E^{0'}$) of -275 mV and an additional [4Fe-4S] cluster with -529 mV [39]. A unique feature of Fdx_sac is the binding of one zinc ion as additional cofactor. *S. acidocaldarius* grows aerobically as a heterotroph and uses PFOR for catabolic pyruvate oxidation. The dual redox clusters in Fdx_sac may reflect a dual function as electron acceptor or electron donor in combination with the different OFORs present in crenarchaeota for heterotrophic and autotrophic growth, respectively. However, the capability of PFORsac to work as pyruvate synthase has not been demonstrated experimentally so far.

Fig. 5 presents the result of the CO_2 fixation assay with PFORdaf in combination with MV as redox mediator. After 30 min incubation, HPLC analysis revealed a peak, that was missing in control experiments and that could be identified as pyruvate semicarbazone by reference compound and mass spectrometry (Fig. 5). These result demonstrate that the applied conditions were convenient for assaying pyruvate synthase *in vitro*.

Results of pairing PFORdaf and PFORsac, respectively, with different electron carriers are given in Table 2 and the kinetics of the reactions are shown in Fig. 6. Because of the stoichiometry of the reaction, the molar amount of formed pyruvate semicarbazone equals the molar amount of fixed CO_2.

No pyruvate semicarbazon product could be detected with Fdx_daf in combination with either enzyme, confirming the expectation that the standard redox potential of this ferredoxin is not sufficiently low to support CO_2 fixation.

This conclusion is also supported by the thermodynamic analysis of Fig. 3, where with $E^{0'}$ = -385 mV, it is virtually impossible to achieve a reduction grade of the redox carrier, low enough to enter the parameter range for CO_2 fixation. Fdx_sol was also only a poor electron donor for PFORdaf.

In contrast, both low-potential electron carriers, Fdx_cte as well as Fdx_sac, allowed *in vitro* CO_2 fixation with both PFOR enzymes. The highest activity was observed with PFORdaf in combination with Fdx_cte.

The limited availability of ferredoxin prevents the determination of kinetic parameters in the present study. All ferredoxins had to be isolated from the natural host organisms and yielded different amounts. Concentrations of the various ferredoxins in the assay were in the µM range whereas commercially available MV could be applied at much higher concentrations of

1 mM. Note also that PFORsac was operated at higher temperature of 70 °C and that no activity could be observed at room temperature with this enzyme in accordance with the temperature optimum of the oxidative MV reduction activity and the hyperthermophilic lifestyle of *S. acidocaldarius*.

Nevertheless, despite this restriction, the data presented demonstrate that both PFORdaf as well as PFORsac can be operated *in vitro* in the CO_2-fixing direction with appropriate electron carriers under the applied conditions.

Generally, the activities of PFORdaf were significantly higher than those obtained with PFORsac, however with one exception: CO_2 fixation with both PFOR enzymes could also be demonstrated in control assays where redox mediators were completely omitted. This finding indicates that the photochemical EDTA/deazaflavin system alone was sufficient to effectively reduce the catalytic Fe-S clusters of the enzymes. The reduction was confirmed by difference absorption spectroscopy for PFORdaf (data not shown). In this case, without any external electron carriers involved, PFORsac activity was more than twice as high as PFORdaf. The results suggest that PFORsac under the applied conditions (70 °C) was more effectively reduced by deazaflavine/EDTA treatment than PFORdaf. However, in contrast to PFORdaf, there was only a small effect on the overall activity of PFORsac by adding ferredoxin or MV as redox mediators.

For PFORdaf, the non-natural redox partner Fdx_ctep was the most efficient electron carrier of all compounds tested, in accordance with the very low midpoint potential of this ferredoxin ($E^{0'}$ = -584 mV). With Fdx_sac, only about 35 % of that activity was obtained. So far, Fdx_sac has only been described as an efficient electron acceptor for the decarboxylating PFOR reaction [40].

As a further result, both enzymes could also be operated using MV (1,1′-dimethyl-4,4′-dipyridinium dichloride. syn. Paraquat) as an artificial electron donor. MV is routinely used as an oxidant in the decarboxylating PFOR assay where the reduction of MV produces a blue-color radical cation ($MV^{+\bullet}$) thus allowing to follow the reaction by absorption spectroscopy. As the results show, photochemically reduced MV was also capable in driving the reverse reductive carboxylation with PFORdaf as well as PFORsac when applied at concentrations of 1 mM. However, MV was not a very efficient electron donor, since lowering the assay concentration of MV to the range of the applied ferredoxins resulted in a lack of any detectable product. In addition, also MV concentrations higher than 1 mM significantly

lowered the CO_2-fixing activities (data not shown). Despite the lower activity, MV might be nevertheless useful as an alternative electron donor for assaying the pyruvate synthase function of PFOR enzymes when a cognate ferredoxin is not available since MV is produced as a low-cost commercial herbicide.

With $E^{0'}$ = -446 mV (Table 1) the redox potential of the MV reduced/oxidized couple is formally not low enough to support CO_2 reduction. Hence, with the relationships of Fig. 3, to achieve a neg. ΔG for the CO_2 reduction by MV theoretically requires a minimal $MV^{+\bullet}/MV^{2+}$ ratio of at ca. 15:1. In other words, the reduced species $MV^{+\bullet}$ should account for more than 93.5 % of total MV. The finding that it was not possible to drive CO_2 fixation with photochemically pre-reduced MV in darkness illustrates that the continuous input of low potential electrons from light-activated EDTA/deazaflavin is essential for maintaining the MV redox potential sufficiently low to drive the reaction.

With Fdx_sol, the required redox ratio is even higher with 49:1 corresponding to a 98 % reduced pool and with Fdx_daf it is virtually impossible to enter the parameter range for CO_2 fixation in Fig. 3. Here, the theoretical minimally required redox ratio of 158:1, i.e. 99.4 % reduced, apparently could not be provided by the reaction system.

With the more reducing Fdx_sac ($\Delta E^{0'}$= -529 mV) and Fdx_cte ($\Delta E^{0'}$= -584 mV), respectively, the CO_2-fixing direction becomes much more accessible. The low midpoint potentials allow to thermodynamically drive the reaction even in a highly oxidized state with only 6.4 % of Fdx_cte and 37 % of Fdx_sac, respectively, have to be in the reduced form. The experimental results are in full agreement with these thermodynamic considerations.

As shown in Fig. 6, after ca. 30 min of incubation, the reaction ceased although all substrates were still present in saturating amounts. Samples of the CO_2-fixing pyruvate synthase assay were taken after several intervals of incubation and then assayed again using the complementary routine MV reduction assay. These experiments showed that the enzyme activity was inversely correlated with accumulating pyruvate semicarbazone. Control experiments confirmed that incubation of PFORdaf in the presence of pyruvate semicarbazone at 50 °C for 90 min completely abolished the MV reducing activity (data not shown). No inhibition of the enzyme was observed after 90 min incubation at assay conditions without addition of pyruvate semicarbazone or incubation with pyruvate semicarbazone at room temperature. It is therefore very likely that accumulating pyruvate semicarbazone in combination with high temperature was the reason for the enzyme inhibition thereby

preventing a longer term operation. With PFORsac the reaction followed a slower and more linear progression and the inhibitory pyruvate semicarbazone concentration was not reached within the one hour assay period (Fig. 6B).

How efficient is CO_2 fixation by PFORdaf?

As outlined above, no detailed kinetic analysis was conducted in the present study. In the following, we attempt to estimate the efficiency of PFORdaf as a CO_2-utilizing pyruvate synthase enzyme, based on theoretical considerations. Determining the exact concentration of CO_2 in the assay is complicated by the fact that CO_2 in aqueous solution undergoes a temperature and pH-dependent equilibrium between the molecular species H_2CO_3, CO_2(aq), HCO^- and CO^{2-}. Since only CO_2(aq) is accepted as substrate by PFOR, the CO_2-water equilibrium has to be considered for estimating the effective available concentration of CO_2. In a *closed system*, at the applied pH 7.2, the HCO^- species dominates and only a smaller molar fraction is present as dissolved CO_2(aq). Hence, with 200 mM $NaHCO_3$ added to the test tube, CO_2(aq) can be estimated according to the Henderson-Hasselbach equation ($pH = pKa + \log(HCO^-/H_2CO_3)$). Using a reported pKa value of 6.35 [41] for the dissociation of $CO_2 + H_2O \leftrightarrow HCO^- + H^+$, the effective concentration of CO_2(aq) would be about 25 mM from added $NaHCO_3$.

However, more important is the additional supply of CO_2 by the gas phase in our assay. In order to prevent loss of CO_2 and to provide oxygen-free conditions, the assay solution was purged with CO_2 in sealed tubes and the assay thus was performed under a CO_2 atmosphere. Therefore, the assay represents an *open system*, where consumed CO_2(aq) is replaced by the gas phase. With the equilibrium assumption, well-known relationships allow a crude estimation of the concentration of dissolved CO_2(aq) here: At 25-30 °C, the Henry's law constant for CO_2, is $K^0_H = 0.034$ M bar^{-1} [42]. With Henry's law, $cCO_2 = K_H \times pCO_2$, the concentration of CO_2(aq) in aqueous solution then would be 34 mM, assuming atmospheric pressure of the CO_2 gas phase. Note that the concentration of dissolved CO_2(aq) is invariant to pH here, because of equilibrium conditions in an open system.

To compensate for the assay temperature (40 °C for PFORdaf, 70 °C for PFORsac), a temperature dependency constant C = 2400 K has to be taken into account [42]. With these parameters, a temperature-dependent Henry's law constant $K_{H(T)}$ can be calculated according to the Van't Hoff equation $K_{H(T)} = K^0_H \exp((C \times ((1/T) - (1/298.15\ K)))$. The resulting concentration of CO_2(aq) using this coefficient for PFORdaf at 40 °C would be 23 mM and 18

mM for PFORsac at 70 °C (Note that these calculations are for pure water and ionic strength of the buffer is neglected).

There are only few data available for the reductive CO_2-fixing operation of PFOR. A previous study reported kinetic parameters for PFOR of *Moorella thermoacetica* (f. *Clostridium thermoaceticum*) (PFORmot) [30]. The structure of PFORmot was recently resolved as a homodimeric protein with high similarity to PFORdaf in the active site and overall domain architecture, except that domain VII is missing [24]. In that study, for PFORmot, a K_m-value for CO_2 of 2.0 mM, has been calculated with the Henderson-Hasselbach equation from added $KHCO_3$ [30]. Further kinetic constants were reported for acetyl-CoA (K_m = 9.1 µM, V_{max} = 1.6 units mg^{-1}, k_{cat} = 3.2 s-1) and ferredoxin (K_m = 0.27 µM, k_{cat} = 2.0 s^{-1}) [30]. It should be noted, that a CO_2-generating enzyme, CO-dehydrogenase, was present in the upstream reaction of that assay which might be a potential source of bias in estimating CO_2(aq).

With respect to the data for PFORmot, all substrates in our present assay are more than 10-fold above the reported K_m values (ferredoxin: 2.8 × 10^{-2} mM vs. 2.7 × 10^{-4} mM; acetyl-CoA: 2.8 mM vs. 9.1 × 10^{-3} mM; CO_2(aq): 23 mM vs. 2.0 mM). With these conditions, all substrates in our test tube are likely to be saturating for the pyruvate synthase reaction. This assumption allows to derive a calculated turnover number for CO_2 for PFORdaf in combination with Fdx_ctep of k_{cat} = 1.4 s^{-1}(with enzyme concentration = 0.7 µM and V_{max} = 60 µM min^{-1}).

Other CO_2-fixing enzymes exhibit similar low turnover numbers. For ribulose-1,5-bisphoshate carboxylase/oxygenase, reported turnover numbers for CO_2, taken from the Brenda database (http://brenda-enzymes.org) differ over a large span from k_{cat} 0.2 $s^{-1}$to 13.9 s^{-1}. The estimated kinetic constants for PFORdaf (as well as PFORsac) operating as pyruvate synthase thus awaits experimental validation in further studies.

The highest activity of the present study with the combination PFORdaf-Fdx_cte (325 nmol min^{-1} mg^{-1}) corresponds to an extrapolated specific productivity of ca. 860 g converted CO_2 h^{-1} g $enzyme^{-1}$. With respect to the substrate, a 53 % conversion of acetyl-CoA was achieved.

In conclusion, the present work is the first experimental demonstration that two PFOR enzymes which in their native host function as pyruvate decarboxylating enzymes can also work in the reverse direction as pyruvate synthases *in vitro*. Although a recent electrochemical study indicated the reductive operation of PFORdaf by cyclic voltammetry

[34], examining the catalytic properties of an enzyme requires a biochemical assay where substrate and product concentrations can be monitored over time.

PFOR enzymes have already been recognized as high potential biocatalysts and some technical applications using the oxidative pyruvate-decarboxylating function have been reported. Recently, immobilized PFOR of *Citrobacter* spec. has been utilized for the production of acetyl-CoA [43]. In another approach, PFORdaf was incorporated *in vivo* in a synthetic hydrogen production pathway in *E. coli* [44].

As the present study points out, PFORs carboxylating pyruvate synthase activity could also be applicable for *in vitro* fixation of CO_2 as well. The recently presented CETCH cycle of Schwander et al. [46] is pioneering in being the first synthetic CO_2 fixation cycle. The cycle, however, does not include PFOR but uses crotonyl-CoA carboxylase/reductase as CO_2-fixing enzyme to yield glyoxylate as end product. In a pathway context, PFOR might offer an interesting alternative perspective for the further development of enzymatic CO_2 conversion. For example, a number of enzymes are known, such as pyruvate carboxylase or malic enzyme, opening a route to C4 compounds, some of which are important platform chemicals, by further addition of CO_2 to pyruvate. Although the *in vitro* reductive CO_2 fixation still requires anaerobic conditions for obtaining a sufficiently low redox potential, the high oxygen stability of both, PFORdaf as well as PFORsac, is of general advantage for purification and storage.

Furthermore, with the biochemical assay presented in this work, the rapid screening of the pyruvate synthase function of PFOR becomes possible for further examination of the intriguing properties of these bifunctional enzymes.

Materials and methods

Organisms and growth conditions

Desulfovibrio africanus (DSM 2603, Campell et al., 1966), *Sulfolobus acidocaldarius* (DSM 639, Brock et al, 1972) and *Chlorobaculum tepidum* (DSM 12025, [45] were cultivated for isolation of ferredoxins and enzymes. *E. coli* Tuner™(DE3) (Merck KGaA, Darmstadt, Germany) and *E. coli* BL21(DE3)Δ*iscR* [33], kind gift from Patrick Jones, Imperial College London) served as expression hosts for heterologous expression of enzymes. *E. coli* XL1-Blue (Agilent, Santa Clara, USA) was involved for cloning procedures.

For anaerobic cultivations with *D. africanus* and *C. tepidum*, hungate flasks were used and the media were purged with CO_2 and N_2 to exclude oxygen. Resazurin was added as redox indicator.

D. africanus was incubated for 2 weeks in the growth medium of the DSMZ-German Collection of Microorganisms and Cell Cultures (DSMZ), No. 63 at 30 °C and 100 rpm in a shaker or on a magnetic stirrer at 30 °C and 120 rpm until the suspension has reached a dark black colour. For cultivation of *S. acidocaldarius*, a modified (5 g/L yeast extract instead of 1 g/L) DSMZ medium No. 88 with 5 g/L yeast extract in 1 L shake-flasks with baffles was employed and after inoculation, incubated at 70 °C and 150 rpm for 72 - 120 h. *C. tepidum* was cultivated at phototrophic anaerobic conditions in hungate-flasks in the mineral growth medium described in [45]. The cultures were incubated at 42 °C and 150 rpm under synthetic light for 5-7 days (Multitron Pro Incubator, Infors AG, Bottmingen, Switzerland).

E. coli strains were cultivated in LB (lysogeny broth) medium in baffeled shake-flask at 37 °C and 150 rpm. in a rotary shaker. Where necessary, the medium was supplemented with appropriate antibiotics (ampicillin (100 µg/ml), kanamycin (50 µg/ml), tetracycline (10 mg/ml)) for selection.

Molecular cloning procedures

PFOR from *D. africanus* (Desaf_2186) was obtained as a 3857 bp synthetic gene (life technologies, Carlsbad, USA) with codon adjustment for expression in *E. coli*. The synthetic gene was inserted in a pET23d plasmid vector to yield a 7354 bp recombinant plasmid pET23d*pfordaf*. The plasmid was chemically transformed into the expression strains *E. coli* Tuner™(DE3) and *E. coli* BL21(DE3)Δ*iscR* [32].

For the PFOR sequence of *S. acidocaldarius*, a respective expression plasmid pET23d*pforsac* was constructed by cloning the native gene. For the construction, a 2.7 kbp fragment was

amplified by PCR from genomic DNA of *S. acidocaldarius*. For genomic DNA isolation, *S. acidocaldarius* was cultivated in modified M88 medium for 72 h. Genomic DNA was isolated from 2 mL culture by phenol/chloroform extraction and RNA digestion was conducted with RNase A.

Primers were designed to clone *pforsac* in frame with a C-terminal His-tag. Oligonucleotides, PFORSac_NcoIfor (5'ATCCATGGGTATAGGTGGACCCCAAGGAC3') and PFORSac_XhoIrev (5'CTCGAGAATCCTTTTAGCTTTTATTAATTCATCTAT3') were used to introduce NcoI and XhoI restriction sites, respectively. The amplified gene was cloned into linearized pET23d by NcoI and XhoI restriction digestion and DNA ligation with T4 DNA Ligase. *E.coli* XL1 Blue was used for propagation of plasmids.

The recombinant plasmid pET23d*pforsac* was transformed into *E. coli* BL21(DE3)Δ*iscR* for protein expression. All constructs were verified by sequencing.

Heterologous expression of PFOR

For PFORdaf expression, 100 ml LB medium shake-flasks without baffels were inoculated with an overnight culture to an optical density at 600 nm (OD_{600}) of 0.1 and then incubated at 37 °C and 150 rpm for 2-3 h until an OD_{600} nm of ~1.2 was reached. Then PFOR expression was induced with 0.5 mM IPTG. The culture was transferred into a hungate-flask and incubated over night at 22 °C and 100 rpm under anaerobic conditions for the expression of enzymatically active PFOR.

For large scale production, a 10 L Biostat Cplus fermentor (Sartorius, Goettingen, Germany) was used and inoculated with 500 ml preculture. Since high oxygen levels during the growth phase had shown a negative impact on the resulting activity of recombinant PFORdaf, the dissolved oxygen was controlled at a low value of 3 % air saturation during the growth phase. When the culture reached an OD_{600} of 2.0 - 2.5, the expression was induced by 0.5 mM IPTG. After the induction, the gassing was stopped and the temperature was lowered 22 °C for anaerobic expression (for around 16 h).

After harvesting, the cell suspension was centrifuged at 4500 × g for 15 min at 4 °C. The cell pellet was resuspended in 50 mM Tris/HCl pH 7.5 and stored at -20 °C until protein purification.

Recombinant PFORsac expression by *E.coli* BL21(DE3)Δ*iscR*pET23d*pforsac* was induced at aerobic conditions at 30 % air saturation since the presence of oxygen did not result in a loss of enzyme activity, here.

Protein purification

Cells of *E. coli* containing recombinant PFORdaf were suspended in 25 mM Tris/HCl buffer pH 7.5 with 300 mM NaCl and disrupted using Bug Buster reagent solution (Merck KGaA, Darmstadt, Germany) or alternatively for large scale cultures with a APV-2000 French Press apparatus (SPX Flow, Charlotte, USA). The cell lysate was centrifuged at 23 000 × g for 30 min and the supernatant then applied to a HisTrap HP 5 ml column with a flow rate of 5 ml min^{-1}. Elution was performed with 25 mM Tris/HCl buffer pH 7.5 containing 300 M NaCl and 500 mM imidazole (step elution with 20% elution buffer over 10 column volumes, then 20-100% gradient over 5 column volumes). PFORdaf fractions were stored at -80°C after concentration and buffer exchange (25 mM Tris/HCl buffer pH 8.0) using Vivaspin 20 filtration tubes (100 kD MWCO).

PFORsac was isolated by immobilized metal affinity chromatography as above with the following modifications: PFORsac fractions were concentrated and desalted using Vivaspin 20 filtration tubes (50 kD MWCO) and then applied to a HiLoad Sepharose Q HP 16/10 column (GE Healthcare, Freiburg, Germany) (3 ml min^{-1}) equilibrated with 25 mM Tris/HCl buffer pH 8.0. Elution was performed with 25 mM Tris/HCl buffer pH 8.0 containing 1 M NaCl (0-100% gradient over 10 column volumes). PFORsac fractions were stored at 4°C after concentration and buffer exchange (25 mM Tris/HCl buffer pH 8.0) using Vivaspin 20 filtration tubes (50 kD MWCO).

Ferredoxins were isolated from the natural hosts by a modification of the strategy described by Yoon et al. [38]. Cells of *C. tepidum* were suspended in 25 mM Tris/HCl buffer pH 8.0 and disrupted using Bug Buster reagent solution (Merck KGaA, Darmstadt, Germany). The cell lysate was centrifuged at 23 000 × g for 30 min and the supernatant applied to a Sepharose Q FF column (1.6x10 cm, 5 ml min^{-1}) (GE Healthcare, Freiburg, Germany). Elution was performed with 25 mM Tris/HCl buffer pH 8.0 containing 1 M NaCl (0-100 % gradient over 10 column volumes). Ferredoxin fractions (detected by absorption at 390 nm) were pooled, diluted with the same volume of equilibration buffer and applied to a second AIEX chromatography (Hiload Sepharose Q HP 16/10, 3 ml min^{-1}) (GE Healthcare, Freiburg, Germany) using the same elution conditions. The resulting two ferredoxin-containing peaks were pooled separately, treated with saturated ammonium sulfate solution to a final concentration of 2.3 M $(NH_4)_2SO_4$ and applied to a HIC Hiload Phenylsepharose HP 16/10 colum (GE Healthcare, Freiburg, Germany), 3 ml min^{-1}, equilibrated with 25 mM Tris/HCl buffer pH 8.0 with 2.3 M $(NH_4)_2SO_4$). Elution was carried out with 25 mM Tris/HCl buffer pH 8.0 (0-100% gradient over 10 column volumes).

Ferredoxins of *C. tepidum* could be isolated as single peaks (data not shown) and after concentration and buffer exchange using Vivaspin 20 filtration tubes, were stored at -80°C. The identity of the ferredoxins was confirmed by mass spectrometry of peptides after tryptic digestion. The same strategy was applied for isolation of ferredoxins from *D. africanus* und *S. acidocaldarius*.

Enzyme assays

The oxidative decarboxylating activity of PFOR was measured colorimetrically using methylviologen as electron acceptor and a glucose oxidase/catalase scavenger system for removal of oxygen. The assay mixture contained 20 mM methyl viologen, 40 mM glucose, 0.5 mM coenzyme A, 20 mM pyruvate and 10 mM thiamin-pyrophosphate in 100 mM Tris/HCl buffer, pH 9.0. Measurements were performed at room temperature in the presence of 1000 U ml^{-1}glucose oxidase and 1000 U ml^{-1} catalase. After starting the reaction by adding enzyme, the assay was covered with water-saturated butanol to avoid oxygen and absorption was followed at 604 nm in a spectrophotometer (Jasco V-560, Jasco, Pfungstadt,Germany) at a temperature of 40 °C for PFORdaf and 70 °C for PFORsac.

For the CO_2-fixing pyruvate synthase assay, an assay mixture containing 12.5 mM EDTA, 0.5 mM deazaflavin, 200 mM $NaHCO_3$ and 100 mM semicarbazide in 25 mM phosphate buffer pH 7.4 was purged with nitrogen and carbon dioxide for 20 minutes and the pH was then re-adjusted to 7.4. Acetyl-coenzyme A (6 µmol) was dissolved in 2 ml assay mixture in Hungate tubes. After addition of enzymes (PFORdaf or PFORsac) and electron-carriers (ferredoxins or methyl viologen), the tubes were closed, evacuated and purged with carbon dioxide. The complete assay volume was 2 ml. The assay tubes were illuminated using a slide projector at a light intensity of 250 - 300 µE measured with a light meter (LI-205A, LI-COR, inc., Nebraska). Samples to follow the conversion were taken with a syringe through the septum of the Hungate tube and analyzed by HPLC (Agilent 1100 series, Agilent Technologies, Waldbronn, Germany).

Chemical and analytical procedures

Deazaflavine (3,10-dimethyl-5-deazaflavine) was synthesized from 6-chloro-3-methyluracil and N-methylaniline in DMF/POCl3 following the procedure of [47]. Pyruvate semicarbazone was prepared from pyruvate and semicarbazide hydrochloride according to [48].

HPLC analysis of pyruvate semicarbazone was performed using a Rezex ROA-Organic Acid column (150 × 4.6 mm) (Phenomenex, Aschaffenburg, Germany) with isocratic elution (5 mM H_2SO_4), 0.15 ml min^{-1}, on an Agilent 1100 chromatography system (Agilent Technologies, Waldbronn, Germany). Pyruvate semicarbazone was detected at 254 nm.

HPLC-MS/MS analysis was performed under analogous conditions, except adding 5% acetonitrile to the eluent, on a Thermo Scientific Ultimate 3000 UHPLC system (Thermo Fisher Scientific Inc., Dreieich, Germany), combined with an LTQ XL, linear ion trap mass spectrometer (Thermo Fisher Scientific Inc., Dreieich, Germany) and electrospray ionization (ESI). ESI source conditions were: capillary temperature, 275 °C; spray voltage, 3.2 kV; sheat gas flow rate, 32. The pyruvate semicarbazone selected reaction monitoring (SRM) fragmentation was detected in positive mode (normalized collision energy, 22; precursor ion, m/z 146, product ion, m/z 103) (Fig. 5).

References

1 Cotton CA, Edlich-Muth C & Bar-Even A (2018). Reinforcing carbon fixation. *Curr Opin Biotechnol* **49,** 49–56.

2 Alissandratos A & Easton CJ (2015). Biocatalysis for the application of CO_2 as a chemical feedstock. *Beilstein J Org Chem* **11,** 2370–2387.

3 Shi J, Jiang Y, Jiang Z, Wang X, Wang X, Zhang S, Han P & Yang C (2015). Enzymatic conversion of carbon dioxide. *Chem Soc Rev* **44,** 5981–6000.

4 Ducat DC & Silver PA (2012). Improving carbon fixation pathways. *Curr Opin Chem Biol* **16,** 337–344.

5 Erb TJ & Zarzycki J (2016). Biochemical and synthetic biology approaches to improve photosynthetic CO_2-fixation. *Curr Opin Chem Biol* **34,** 72–79.

6 Claassens NJ (2017). A warm welcome for alternative CO_2 fixation pathways in microbial biotechnology. *Microb Biotechnol* **10,** 31–34.

7 Gibson MI, Chen PY-T & Drennan CL (2016). A structural phylogeny for understanding 2-oxoacid oxidoreductase function. *Curr Opin Struct Biol* **41,** 54–61.

8 Berg IA, Ramos-Vera WH, Petri A, Huber H & Fuchs G (2010). Study of the distribution of autotrophic CO_2 fixation cycles in Crenarchaeota. *Microbiology* **156,** 256–269.

9 Pineda E, Encalada R, Rodriguez-Zavala JS, Olivos-Garcia A, Moreno-Sanchez R & Saavedra E (2010). Pyruvate:ferredoxin oxidoreductase and bifunctional aldehyde-alcohol dehydrogenase are essential for energy metabolism under oxidative stress in *Entamoeba histolytica*. *FEBS J* **277,** 3382–3395.

10 Song H-O (2016). Influence of 120 kDa Pyruvate:Ferredoxin Oxidoreductase on Pathogenicity of *Trichomonas vaginalis*. *Korean J Parasitol* **54,** 71–74.

11 Brostedt E & Nordlund S (1991). Purification and partial characterization of a pyruvate oxidoreductase from the photosynthetic bacterium *Rhodospirillum rubrum* grown under nitrogen-fixing conditions. *Biochem J* **279 (Pt 1),** 155–158.

12 Noth J, Krawietz D, Hemschemeier A & Happe T (2013). Pyruvate:ferredoxin oxidoreductase is coupled to light-independent hydrogen production in *Chlamydomonas reinhardtii*. *J Biol Chem* **288,** 4368–4377.

13 Evans MC, Buchanan BB & Arnon DI (1966). A new ferredoxin-dependent carbon reduction cycle in a photosynthetic bacterium. *Proc Natl Acad Sci U S A* **55,** 928–934.

14 Fuchs G (2011). Alternative pathways of carbon dioxide fixation. *Annu Rev Microbiol* **65,** 631–658.

15 Erb TJ (2011). Carboxylases in natural and synthetic microbial pathways. *Appl Environ Microbiol* **77,** 8466–8477.

16 Boyle NR & Morgan JA (2011). Computation of metabolic fluxes and efficiencies for biological carbon dioxide fixation. *Metab Eng* **13,** 150–158.

17 Fontecave M (2006). Iron-sulfur clusters. *Nat Chem Biol* **2,** 171–174.

18 Ragsdale SW (2003). Pyruvate ferredoxin oxidoreductase and its radical intermediate. *Chem Rev* **103,** 2333–2346.

19 Yan Z, Maruyama A, Arakawa T, Fushinobu S & Wakagi T (2016). Crystal structures of archaeal 2-oxoacid:ferredoxin oxidoreductases from *Sulfolobus tokodaii*. *Sci Rep* **6,** 33061.

20 Chabriere E, Charon MH, Volbeda A, Pieulle L, Hatchikian EC & Fontecilla-Camps JC (1999). Crystal structures of the key anaerobic enzyme pyruvate:ferredoxin oxidoreductase, free and in complex with pyruvate. *Nat Struct Biol* **6,** 182–190.

21 Pieulle L, Guigliarelli B, Asso M, Dole F, Bernadac A & Hatchikian EC (1995). Isolation and characterization of the pyruvate-ferredoxin oxidoreductase from the sulfate-reducing bacterium *Desulfovibrio africanus*. *Biochim Biophys Acta* **1250,** 49–59.

22 Hatchikian EC, Cammack R, Patil DS, Robinson AE, Richards AJM, George S & Thomson AJ (1984). Spectroscopic characterization of ferredoxins I and II from *Desulfovibrio africanus*. *Biochim Biophys Acta* **784,** 40–47.

23 Pieulle L, Magro V & Hatchikian EC (1997). Isolation and analysis of the gene encoding the pyruvate-ferredoxin oxidoreductase of *Desulfovibrio africanus*, production of the recombinant enzyme in *Escherichia coli*, and effect of carboxy-terminal deletions on its stability. *J Bacteriol* **179,** 5684–5692.

24 Chen PY-T, Aman H, Can M, Ragsdale SW & Drennan CL (2018). Binding site for coenzyme A revealed in the structure of pyruvate:ferredoxin oxidoreductase from *Moorella thermoacetica*. *Proc Natl Acad Sci U S A* **115,** 3846–3851.

25 Chen L, Brugger K, Skovgaard M, Redder P, She Q, Torarinsson E, Greve B, Awayez M, Zibat A, Klenk H-P & Garrett RA (2005). The genome of *Sulfolobus acidocaldarius*, a model organism of the Crenarchaeota. *J Bacteriol* **187,** 4992–4999.

26 Brock TD, Brock KM, Belly RT & Weiss RL (1972). Sulfolobus: a new genus of sulfur-oxidizing bacteria living at low pH and high temperature. *Arch Mikrobiol* **84,** 54–68.

27 Berg IA, Kockelkorn D, Buckel W & Fuchs G (2007). A 3-hydroxypropionate/4-hydroxybutyrate autotrophic carbon dioxide assimilation pathway in Archaea. *Science* **318,** 1782–1786.

28 Neuer G & Bothe H (1982). The pyruvate: ferredoxin oxidoreductase in heterocysts of the cyanobacteriuim *Anabaena cylindric*a. *Biochim Biophys Acta* **716,** 358–365.

29 Yoon K-S, Ishii M, Kodama T & Igarashi Y (2014). Carboxylation Reactions of Pyruvate. *Biosci Biotechnol Biochem* **61,** 510–513.

30 Furdui C & Ragsdale SW (2000). The role of pyruvate ferredoxin oxidoreductase in pyruvate synthesis during autotrophic growth by the Wood-Ljungdahl pathway. *J Biol Chem* **275,** 28494–28499.

31 Ikeda T, Yamamoto M, Arai H, Ohmori D, Ishii M & Igarashi Y (2010). Enzymatic and electron paramagnetic resonance studies of anabolic pyruvate synthesis by pyruvate. *FEBS J* **277,** 501–510.

32 Akhtar MK & Jones PR (2008). Deletion of iscR stimulates recombinant clostridial Fe-Fe hydrogenase activity and H_2-accumulation in *Escherichia coli* BL21(DE3). *Appl Microbiol Biotechnol* **78,** 853–862.

33 Schwartz CJ, Giel JL, Patschkowski T, Luther C, Ruzicka FJ, Beinert H & Kiley PJ (2001). IscR, an Fe-S cluster-containing transcription factor, represses expression of *Escherichia coli* genes encoding Fe-S cluster assembly proteins. *Proc Natl Acad Sci U S A* **98,** 14895–14900.

34 Li B & J. Elliott S (2016). The catalytic cias of 2-oxoacid: ferredoxin oxidoreductase in CO_2: evolution and reduction through a ferredoxin-mediated electrocatalytic assay. *Electrochim Acta* **199**.

35 Flamholz A, Noor E, Bar-Even A & Milo R (2012). eQuilibrator--the biochemical thermodynamics calculator. *Nucleic Acids Res* **40,** D770-5.

36 Bothe H & Neuer G. Electron donation to nitrogenase in heterocysts. In *Methods in Enzymology : Cyanobacteria,* pp. 496–501. Academic Press.

37 Pino T & Cordes EH (1971). Kinetics and mechanism for pyruvic acid semicarbazone formation. *J Org Chem* **36,** 1668–1670.

38 Yoon KS, Bobst C, Hemann CF, Hille R & Tabita FR (2001). Spectroscopic and functional properties of novel 24Fe-4S cluster-containing ferredoxins from the green sulfur bacterium *Chlorobium tepidum*. *J Biol Chem* **276,** 44027–44036.

39 Breton JL, Duff JLC, Butt JN, Armstrong FA, George SJ, Pétillot Y, Forest E, Schäfer G & Thomson AJ (1995). Identification of the iron-sulfur clusters in a ferredoxin from the archaeon *Sulfolobus acidocaldariu*s. *Eur J Biochem* **233,** 937–946.

40 Kerscher L, Nowitzki S & Oesterhelt D (1982). Thermoacidophilic archaebacteria contain bacterial-type ferredoxins acting as electron acceptors of 2-oxoacid:ferredoxin oxidoreductases. *Eur J Biochem* **128,** 223–230.

41 Holleman AF, Wiberg E, Wiberg N & Fischer G (2017) Anorganische Chemie. De Gruyter, Berlin, Boston.

42 Sander R (2015). Compilation of Henry's law constants (version 4.0) for water as solvent. *Atmos Chem Phys* **15,** 4399–4981.

43 Takenaka M, Yoon K-S, Matsumoto T & Ogo S (2017). Acetyl-CoA production by encapsulated pyruvate ferredoxin oxidoreductase in alginate hydrogels. *Bioresour Technol* **227,** 279–285.

44 Agapakis CM & Silver PA (2010). Modular electron transfer circuits for synthetic biology. *Bioeng Bugs* **1,** 413–418.

45 Wahlund TM, Woese CR, Castenholz RW & Madigan MT (1991). A thermophilic green sulfur bacterium from New Zealand hot springs, *Chlorobium tepidum* sp. nov. *Arch Microbiol* **156,** 81–90.

46 Schwander T, Schada von Borzyskowski L, Burgener S, Cortina NS & Erb TJ (2016). A synthetic pathway for the fixation of carbon dioxide in vitro. *Science* **354,** 900-904.

47. Yoneda F, Mori K, Sakuma Y & Koshiro A (1982). Synthesis of some 8-substituted 5-deazaflavins. *J Heterocycl Chem* **19,** 945–947.

48 Bradbury AF & Smyth DG (1987). Enzyme-catalysed peptide amidation. Isolation of a stable intermediate formed by reaction of the amidating enzyme with an imino acid. *Eur J Biochem* **169,** 579–584.

Tables

Table 1. Sources and standard redox potentials $E^{0'}$ (relative to the standard hydrogen electrode) of reductants employed in the present study.

Source	Redox centers	$E^{0'}$ (mV)	Reference
C. tepidum (Fdx_cte)			
FdxI	[4Fe-4S]	-514	Yoon et al., 2001
	[4Fe-4S]	-584	Yoon et al., 2001
D. africanus (Fdx_daf)			
FdxI	[4Fe-4S]	-385	Hatchikian et al., 1984
FdxII	[4Fe-4S]	-385	Hatchikian et al., 1984
FdxIII	[3Fe-4S]	-140	Armstrong et al., 1989
	[4Fe-4S]	- 410	Armstrong et al., 1989
S. acidocaldarius (Fdx_sac)			
Fdx	[3Fe-4S]	-275	Breton et al., 1995
	[4Fe-4S]	-529	Breton et al., 1995
S. oleracea			Cammack et al., 1977
Fdx		-415	
	[2Fe-2S]		
Methylviologen (MV)		-446	Mayhew, 1978

Table 2. Specific pyruvate synthase activities based on formed pyruvate semicarbazone for PFORdaf and PFORsac, respectively with different electron carriers. PFORsac was assayed at 70 °C. -: no activity; n.d.: not determined; neg. control: no electron carrier added.

Electron carrier	Specific activity (nmol*min^{-1} mg^{-1})	
	PFORdaf	PFORsac
Fdx_daf	-	n.d.
Fdx_sac	184.3 ± 32	96.6 ± 11
Fdx_cte	325.0 ± 77	93.7 ± 4.5
Fdx_sol	29.2 ± 11	n.d.
MV	206.2 ± 19	104.7 ± 5.8
neg. control	27.4 ± 5.8	64.0 ± 3.4

Figure legends

Fig. 1. Protomer structures and domain arrangement of PFORdaf (A) and PFORsac (B). Domains: I (green); II (yellow); III (magenta); IV (grey); V (blue); VI (cyan); VII (red). Ligands ([4Fe-4S], TPP-Mg2+) are magnified as ball and stick model and placed in the front for clarity. Atom colors: carbon - grey; nitrogen - blue; oxygen - red; phosphorous - orange; magnesium - green; sulfur: yellow, and iron: brown.

Fig. 2. Heterologous expression of PFORdaf in bioreactor cultures. Left: relative activity of the methylviologen-reduction assay in cell lysates of *E. coli* Tuner (DE3) (light blue column) and *E. coli* BL21(DE3)Δ*iscR* (purple column). Values represent mean of three experiments with standard deviation as error bars. Right: SDS-PAGE of purification of recombinant PFORdaf and PFORsac from bioreactor cultivations. M: marker; 1: cell lysate, PFORdaf; 2: IMAC fraction, PFORdaf; 3: cell lysate, PFORsac; 4: IMAC fraction, PFORsac; 5: AIEX fraction, PFORsac. The band in lane 2 corresponds to the 130 kDa subunit uf homodimeric PFORdaf. Lane 5 shows the 70 kDa α-subunit and 34 kDa β-subunit of heterodimeric PFORsac.

Fig. 3. Gibbs free energy (in kJ/mol) for different standard redox potentials ($E^{0'}$) and reduction states of cofactors. The black line indicates the isocline for the reductive PFOR reaction without redox cofactor consideration (ΔG = 99.5 kJ/mol). The overall CO_2-fixing reaction is infeasible in the parameter space left of the isocline and feasible in the region right to the isocline.

Fig. 4. Reaction scheme of the PFOR reductive carboxylation (pyruvate synthase) assay

Fig. 5. Analysis of the PFOR reductive carboxylation assay by HPLC and ESI-MS/MS. Arrow and structure insert mark the pyruvate semicarbazone product. A: complete assay; B: control, acetyl-CoA omitted; C: control, enzyme omitted; D: ESI-MS/MS analysis by selected reaction monitoring in positive mode, applying the transition from m/z 146 (parent ion) to m/z 103 (product ion); E: fragmentation pattern of pyruvate semicarbazone reference compound where m/z 145.92 corresponds to $[M+H^+]^+$ and m/z 102.92 corresponds to the decarboxylated fragment $[M-44+H^+]^+$.

Fig. 6. Kinetics of pyruvate semicarbazone formation by PFORdaf and PFORsac with different redox mediators. A: PFORsac; B: PFORdaf. Data represent means of three independent determinations with standard deviation as error bars. Legend shown in panel A applies for both panel A and panel B.

Acknowledgments

This work was supported by the German Ministry of Research and Education within the strategy process “Biotechnology2020+” as grant no. 031A180A. We also would like to thank the following undergraduate students for their valuable contributions during their thesis work: Benjamin Kohler, Sven Goral, Fabian Hilzinger, Yujia Liu.

Author contributions

AW isolated ferredoxins and enzymes and conducted enzyme assays and chemical analyses. RP constructed cloning and expression vectors and recombinant strains. SD cultivated strains and characterized enzymes. OH performed computational thermodynamic analyses. HG designed the study and wrote the paper with contributions of all other authors.

Conflict of interest

The authors declare no conflict of interest.

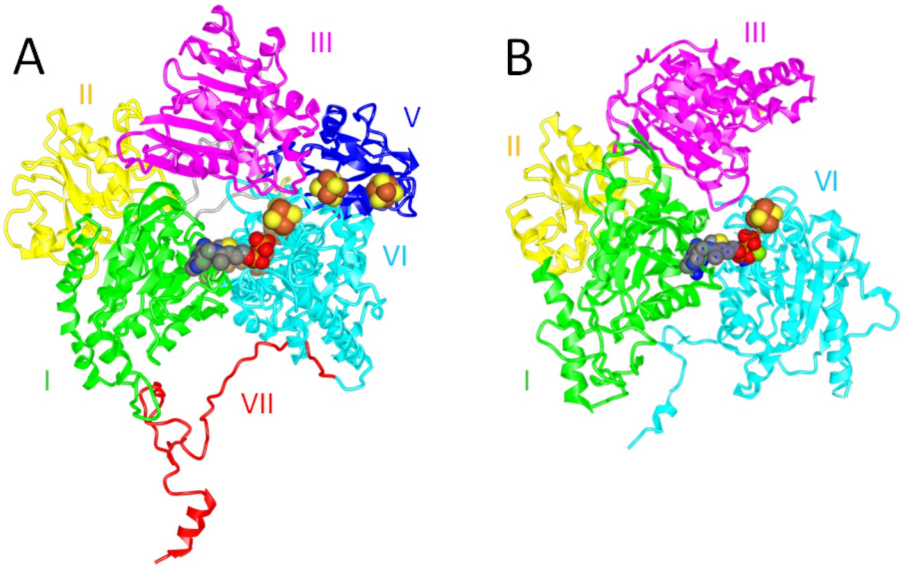

Fig. 1. Protomer structures and domain arrangement of PFORdaf (A) and PFORsac (B). Domains: I (green); II (yellow); III (magenta); IV (grey); V (blue); VI (cyan); VII (red). Ligands ([4Fe-4S], TPP-Mg2+) are magnified as ball and stick model and placed in the front for clarity. Atom colors: carbon - grey; nitrogen - blue; oxygen - red; phosphorous - orange; magnesium - green; sulfur: yellow, and iron: brown.

165x101mm (150 x 150 DPI)

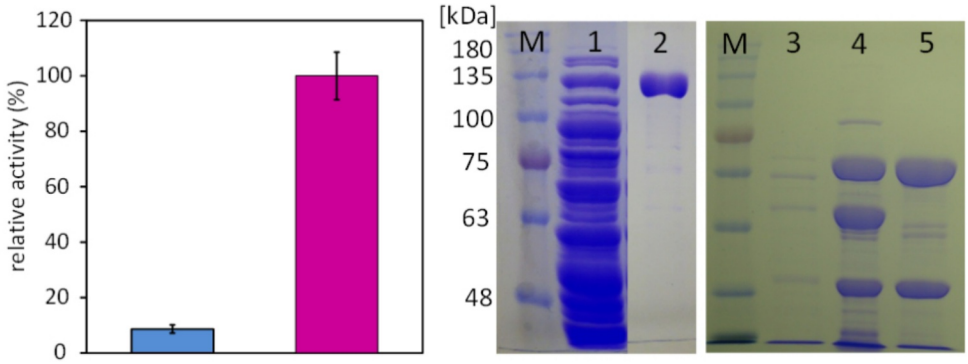

Fig. 2. Heterologous expression of PFORdaf in bioreactor cultures. Left: relative activity of the methylviologen-reduction assay in cell lysates of *E. coli* Tuner (DE3) (light blue column) and *E. coli* BL21(DE3)Δ*iscR* (purple column). Values represent mean of three experiments with standard deviation as error bars. Right: SDS-PAGE of purification of recombinant PFORdaf and PFORsac from bioreactor cultivations. M: marker; 1: cell lysate, PFORdaf; 2: IMAC fraction, PFORdaf; 3: cell lysate, PFORsac; 4: IMAC fraction, PFORsac; 5: AIEX fraction, PFORsac. The band in lane 2 corresponds to the 130 kDa subunit uf homodimeric PFORdaf. Lane 5 shows the 70 kDa α-subunit and 34 kDa β-subunit of heterodimeric PFORsac.

80x32mm (300 x 300 DPI)

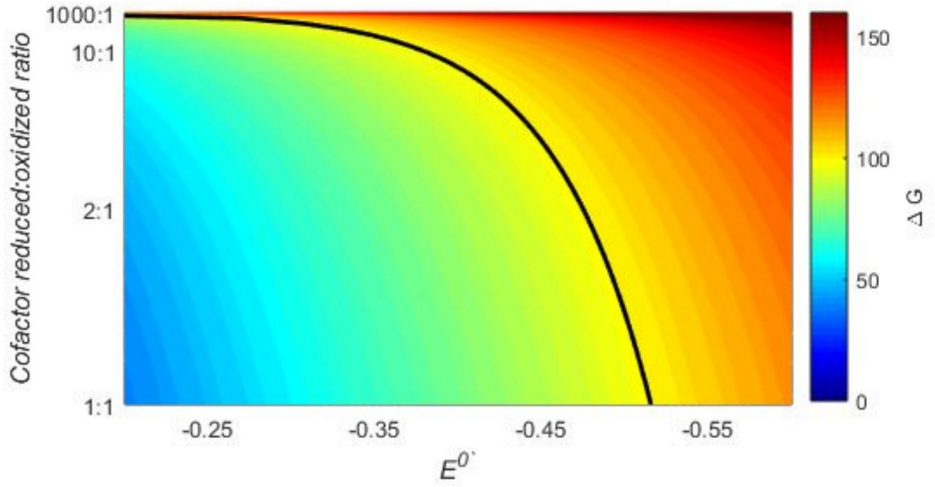

Fig. 3. Gibbs free energy (in kJ/mol) for different standard redox potentials ($E^{0\prime}$) and reduction states of cofactors. The black line indicates the isocline for the reductive PFOR reaction without redox cofactor consideration (ΔG = 99.5 kJ/mol). The overall CO_2-fixing reaction is infeasible in the parameter space left of the isocline and feasible in the region right to the isocline.

148x78mm (96 x 96 DPI)

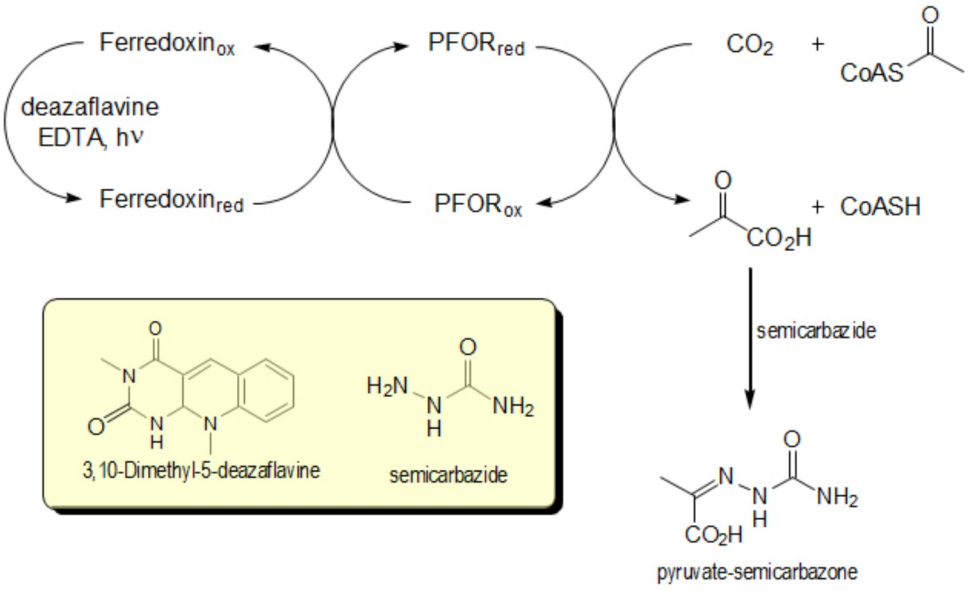

Fig. 4. Reaction scheme of the PFOR reductive carboxylation (pyruvate synthase) assay

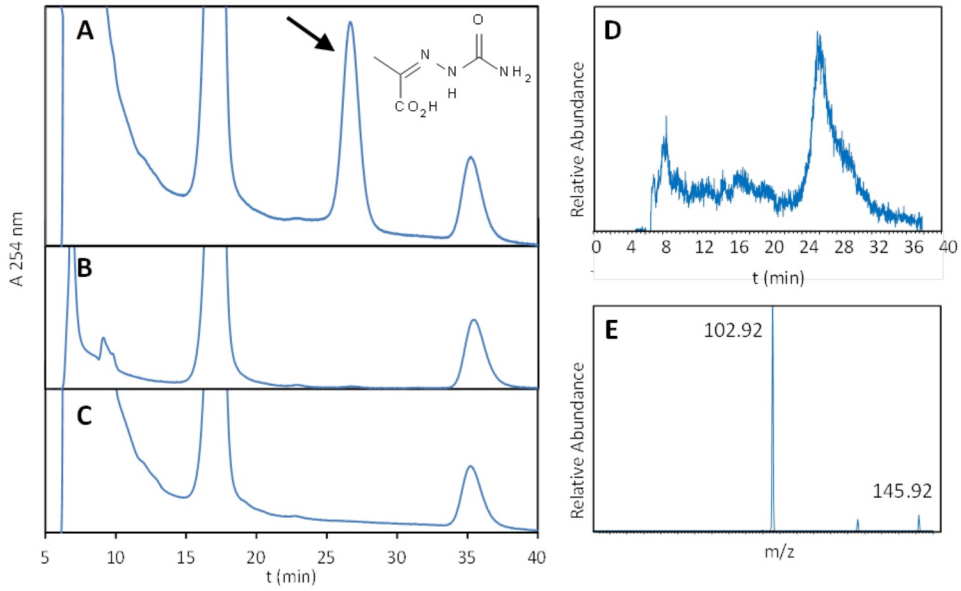

Fig. 5. Analysis of the PFOR reductive carboxylation assay by HPLC and ESI-MS/MS. Arrow and structure insert mark the pyruvate semicarbazone product. A: complete assay; B: control, acetyl-CoA omitted; C: control, enzyme omitted; D: ESI-MS/MS analysis by selected reaction monitoring in positive mode, applying the transition from m/z 146 (parent ion) to m/z 103 (product ion); E: fragmentation pattern of pyruvate semicarbazone reference compound where m/z 145.92 corresponds to $[M+H^+]^+$ and m/z 102.92 corresponds to the decarboxylated fragment $[M-44+H^+]^+$.

164x102mm (150 x 150 DPI)

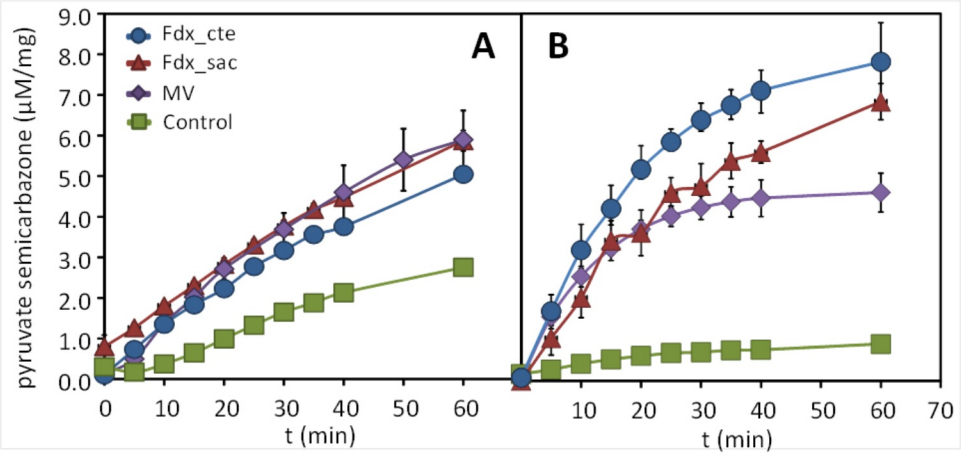

Kinetics of pyruvate semicarbazone formation by PFORdaf and PFORsac with different redox mediators. A: PFORsac; B: PFORdaf. Data represent means of three independent determinations with standard deviation as error bars.

165x81mm (150 x 150 DPI)